Biomedical Optics EXPRESS

Spectral imaging using forward-viewing spectrally encoded endoscopy

Adel Zeidan and Dvir Yelin*

Faculty of Biomedical Engineering, Technion—Israel Institute of Technology, Haifa 3200003, Israel
*yelin@bm.technion.ac.il

Abstract: Spectrally encoded endoscopy (SEE) enables miniature, small-diameter endoscopic probes for minimally invasive imaging; however, using the broadband spectrum to encode space makes color and spectral imaging nontrivial and challenging. By careful registration and analysis of image data acquired by a prototype of a forward-viewing dual channel spectrally encoded rigid probe, we demonstrate spectral and color imaging within a narrow cylindrical lumen. Spectral imaging of calibration cylindrical test targets and an *ex-vivo* blood vessel demonstrates high-resolution spatial-spectral imaging with short (10 μs/line) exposure times.

OCIS codes: (170.2150) Endoscopic imaging; (060.2350) Fiber optics imaging; (070.4790) Spectrum analysis; (330.1690) Color.

References and links

1. G. J. Tearney, M. Shishkov, and B. E. Bouma, "Spectrally encoded miniature endoscopy," Opt. Lett. **27**(6), 412–414 (2002).
2. D. Yelin, I. Rizvi, W. M. White, J. T. Motz, T. Hasan, B. E. Bouma, and G. J. Tearney, "Three-dimensional miniature endoscopy," Nature **443**(7113), 765 (2006).
3. D. Yelin, B. E. Bouma, and G. J. Tearney, "Volumetric sub-surface imaging using spectrally encoded endoscopy," Opt. Express **16**(3), 1748–1757 (2008).
4. D. Yelin, B. E. Bouma, J. J. Rosowsky, and G. J. Tearney, "Doppler imaging using spectrally-encoded endoscopy," Opt. Express **16**(19), 14836–14844 (2008).
5. D. Yelin, B. E. Bouma, S. H. Yun, and G. J. Tearney, "Double-clad fiber for endoscopy," Opt. Lett. **29**(20), 2408–2410 (2004).
6. A. Abramov, L. Minai, and D. Yelin, "Multiple-channel spectrally encoded imaging," Opt. Express **18**(14), 14745–14751 (2010).
7. G. Engel, H. Genish, M. Rosenbluh, and D. Yelin, "Dual-channel spectrally encoded endoscopic probe," Biomed. Opt. Express **3**(8), 1855–1864 (2012).
8. A. Zeidan and D. Yelin, "Miniature forward-viewing spectrally encoded endoscopic probe," Opt. Lett. **39**(16), 4871–4874 (2014).
9. D. Kang, D. Yelin, B. E. Bouma, and G. J. Tearney, "Spectrally-encoded color imaging," Opt. Express **17**(17), 15239–15247 (2009).
10. N. Gat, "Imaging spectroscopy using tunable filters: a review," in *AeroSense 2000*, International Society for Optics and Photonics, 50–64 (2000).
11. M. B. Sinclair, J. A. Timlin, D. M. Haaland, and M. Werner-Washburne, "Design, construction, characterization, and application of a hyperspectral microarray scanner," Appl. Opt. **43**(10), 2079–2088 (2004).
12. Y. Bar-Ilan and D. Yelin, "Spectral imaging using single-axis spectrally dispersed illumination," Opt. Lett. **39**(17), 5177–5179 (2014).
13. A. A. Bunaciu, Ş. Fleschin, and H. Y. Aboul-Enein, "Biomedical Investigations Using Fourier Transform-Infrared Microspectroscopy," Crit. Rev. Anal. Chem. **44**(3), 270–276 (2014).
14. A. Chung, S. Karlan, E. Lindsley, S. Wachsmann-Hogiu, and D. L. Farkas, "In vivo cytometry: A spectrum of possibilities," Cytometry A **69**(3), 142–146 (2006).
15. S. C. Gebhart, R. C. Thompson, and A. Mahadevan-Jansen, "Liquid-crystal tunable filter spectral imaging for brain tumor demarcation," Appl. Opt. **46**(10), 1896–1910 (2007).
16. R. T. Kester, N. Bedard, L. Gao, and T. S. Tkaczyk, "Real-time snapshot hyperspectral imaging endoscope," J. Biomed. Opt. **16**(5), 056005 (2011).
17. C. M. Lee, C. J. Engelbrecht, T. D. Soper, F. Helmchen, and E. J. Seibel, "Scanning fiber endoscopy with highly flexible, 1 mm catheterscopes for wide-field, full-color imaging," J. Biophotonics **3**(5-6), 385–407 (2010).

#254022 Received 16 Nov 2015; revised 27 Dec 2015; accepted 4 Jan 2016; published 8 Jan 2016

18. E. J. Seibel, R. E. Carroll, J. A. Dominitz, R. S. Johnston, C. D. Melville, C. M. Lee, S. M. Seitz, and M. B. Kimmey, "Tethered capsule endoscopy, a low-cost and high-performance alternative technology for the screening of esophageal cancer and Barrett's esophagus," IEEE Trans. Biomed. Eng. **55**(3), 1032–1042 (2008).
19. Y. Hamamoto, T. Endo, K. Nosho, Y. Arimura, M. Sato, and K. Imai, "Usefulness of narrow-band imaging endoscopy for diagnosis of Barrett's esophagus," J. Gastroenterol. **39**(1), 14–20 (2004).
20. A. Abramov, L. Minai, and D. Yelin, "Spectrally encoded spectral imaging," Opt. Express **19**(7), 6913–6922 (2011).
21. H. S. Fairman, M. H. Brill, and H. Hemmendinger, "How the CIE 1931 color-matching functions were derived from Wright-Guild data," Color Res. Appl. **22**(1), 11–23 (1997).
22. M. Anderson, S. Chandrasekar, R. Motta, and M. Stokes, "A standard default color space for the internet: srgb," Technical report, International Color Consortium (1996).
23. S. Prahl, "Optical absorption of hemoglobin," Oregon Medical Laser Center, *http://omlc.ogi.edu/spectra/hemoglobin/index.html* **15** (1999).

1. Introduction

Utilizing spatial wavelength encoding and single-axis scanning, spectrally encoded endoscopy (SEE) [1] enables miniature endoscopy with various potential applications in minimally invasive clinical imaging. SEE with high number of resolvable points have been demonstrated capable of three-dimensional [2], subsurface [3] and Doppler [4] imaging through flexible, single-fiber probes. Reduced speckle noise and increased depth-of-field were achieved using a dual-clad fiber [5] or using separate illumination and collection channels [6, 7]. Recently, we have designed a forward-viewing SEE probe [8] that overcomes some of the limitations of side-viewing probes [2, 9], potentially allowing practical navigation through narrow passages and ducts. Yet, the use of wavelength to encode space prevents SEE from straightforward color imaging, as only a narrow spectral band is detected from each sample location at any given time. Color SEE was enabled by illumination with separate blue, green and red spectral bands [9], and by taking advantage of the continuous linear motion of the probe with respect to the tissue [7]. For many clinical applications, however, color imaging is insufficient for characterizing the imaged tissue; mapping the full optical spectrum emitted from a specimen would provide invaluable information about its function and composition. Previously demonstrated approaches for spectral imaging utilize tunable bandpass filters [10], point-by-point and line scanning [11], spectrally dispersed illumination [12] and interferometric Fourier transform spectroscopy [13]. Minimally invasive hyperspectral imaging was demonstrated using fiber bundle endoscopy with a wavelength swept source [14], a liquid-crystal tunable filter [15] and image mapping using a prism [16]. Hyperspectral endoscopes were also demonstrated using rapid distal fiber scanning [17, 18] and narrow band imaging through various bandpass filters [19].

Spectral imaging using spectral encoding was first demonstrated as a proof of concept on a benchtop system by means of two-dimensional lateral scanning of the spectrally encoded line across a flat specimen [20]. Here, we demonstrate spectral imaging through a forward-viewing miniature probe propagating within a narrow lumen having a cylindrical geometry. As the probe is rotated around its axis and advanced through the lumen, reflections from each location on the inner walls are collected and spatially registered for recording the full spectral image of the target. Following system calibration and characterization using resolution and color test targets, the potential of the system for imaging tissue was demonstrated by *ex-vivo* imaging within a turkey artery, revealing spatial features with the spectral characteristics of oxyhemoglobin.

2. Setup

The design and construction of our forward-viewing separate-channel SEE probe was described in detail in a previous publication [8]. Briefly, the illumination channel (Fig. 1) comprised of a low-coherence supercontinuum laser-driven light source (LDLS Eq. (-99)FC, Energetiq Technology, Inc.) and a 200-μm-diameter core fiber (FG200LCC, Thorlabs Inc.) with a distal end polished at 40° angle for off-axis illumination of the sample. The imaging

#254022 Received 16 Nov 2015; revised 27 Dec 2015; accepted 4 Jan 2016; published 8 Jan 2016

channel consisted (components ordered from the distal to the proximal end) of an SF-66 glass prism with a front surface polished at 18.1°, a laser-cut 1-mm-diameter transmission diffraction grating (1379 lines/mm), a second SF-66 prism, a gradient-index lens, a silica spacer, and a small-core single-mode optical fiber (S460HP, Thorlabs Inc.). The imaging optics were aligned and glued inside a semi-cylinder brass holder with 1 mm inner diameter and a 0.4 mm wall thickness resulting in a probe with an overall diameter of 1.8 mm. The resulted spectrally encoded line had the shortest wavelength encoding a location nearly parallel to the main optical axis of the probe, while the longest wavelength encoding locations at an angle of approximately 27° with respect to the main probe axis. The illumination fiber was attached to the bottom of the brass holder (see Fig. 1(a), inset), so that the illumination spot and the spectrally encoded line overlap in space at a distance of approximately 7 mm from the distal end. Light scattered back from the sample was collected by the imaging channel and transmitted to a home-built spectrometer that comprised of a collimating achromatic lens, a 1379 lines/mm transmission grating, a 50 mm focal length achromatic lens, and a high-sensitivity EMCCD (DU970N-BV, Andor Technology plc.). The SEE probe was packaged within a rigid tube (2.3 mm outer diameter) that was stabilized using ball bearing to prevent off-axis motion. Rotational scanning of the tube was obtained using a stepper motor (StepperStick Motor, All Motion Inc.) in back-and-forth ± 360° rotation angle (Fig. 1(b), Visualization 1). The imaged samples were mounted on a computer-controlled linear translation stage and step-scanned in the z-axis during probe rotation. Reflections from the spectrally encoded lines were recorded by the spectrometer with minimum exposure time of 10 μs/line; however, data transfer was considerably slower at 4.4 ms/line, limited only by the camera read rate. Image data was transformed from polar to Cartesian coordinates for obtaining the true cylindrical field of view [8]. The longest 700 nm and the shortest 400 nm wavelengths encoded the outer (proximal) and inner (distal) circles of the cylindrical field-of-view, respectively (Fig. 1(c)); note, however, that some of the blue wavelengths (400-440) were used to encode angles that would not coincide with the walls of a perfect parallel cylinder (Fig. 1(c)).

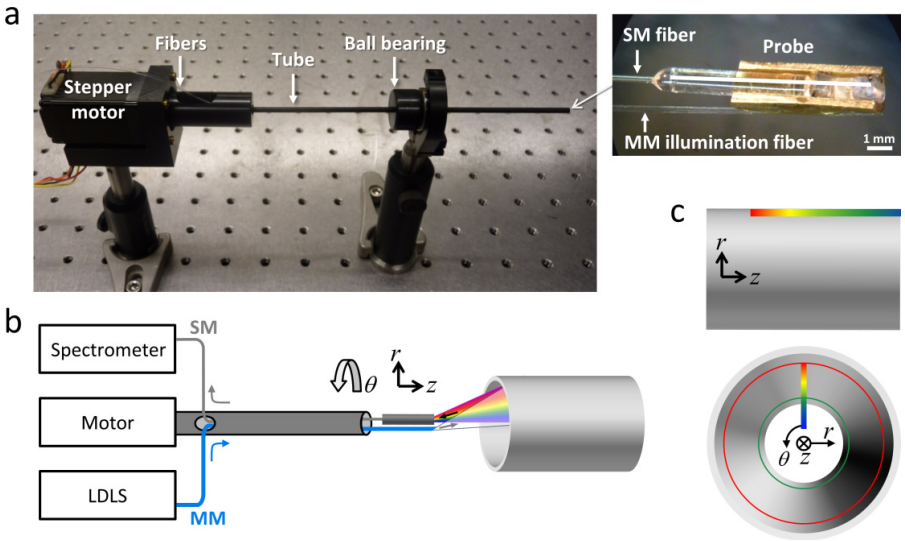

Fig. 1. (a) A photo of the benchtop SEE setup. Inset: high-magnification view of the probe. (b) Schematic illustration of the system. (c) Schematic side and front views of the spectrally encoded line relative to the imaged cylinder. MM - Multimode fiber; SM - Single-mode fiber.

#254022 Received 16 Nov 2015; revised 27 Dec 2015; accepted 4 Jan 2016; published 8 Jan 2016

3. Imaging

In order to demonstrate imaging within a cylindrical sample, a USAF resolution target (Fig. 2, top-left corner) was printed on a white paper and rolled into a 4.5-mm-diameter cylinder. The cylindrical test target was mounted onto a linear translation stage (M-664.164, Physik Instrumente) and scanned along its main (z) axis at small 300-μm discrete steps. Selected frames from the composite movie (Visualization 2) are shown in Fig. 2, each comprised of 1600 spectrally encoded lines with 10 μs/line exposure times. Note the gradual change in the apparent size of the features within the target as the probe advances through the target (Fig. 2, the digits '2' and '4' are marked by arrows). High-magnification view of a selected region of interest (Fig. 2, bottom-right corner) reveals speckle contrast of approximately 0.12 owing to the finite 200 μm diameter of the illumination fiber. The field-of-view of each revolution of the probe was approximately 140 mm^2 (4.5 mm diameter, 10-mm-long cylinder). The lateral resolution (and local contrast) was approximately 100 μm (50%), 8 μm (62%), and 45 μm (41%) for the innermost, middle and outermost circular regions of the field of view, respectively; these variations were caused mainly by the limited 4-mm Rayleigh range of the imaging optics and the difference in geometry between the focal plane and the cylindrical target.

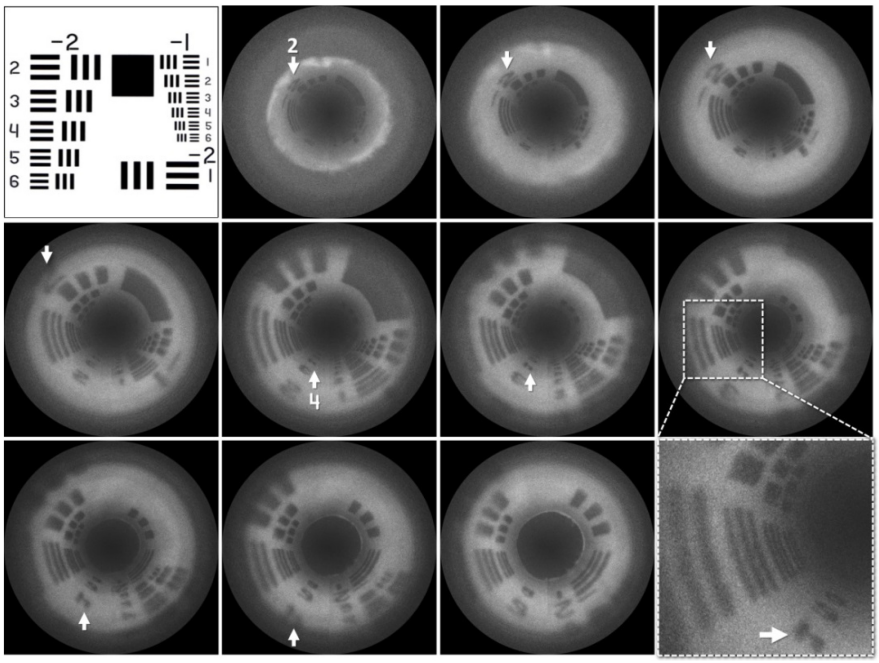

Fig. 2. A series of images acquired with the SEE forward-viewing probe during probe rotation and axial forward motion through a cylindrical test target. The axial step size between the images (left to right, top to bottom) is 1.5 mm. Top-left corner: the test pattern that was printed and rolled into a 4.5 mm diameter cylinder. Bottom-right corner: a high-magnification view of a region of interest marked by dashed square. White arrows point to the digits '2' and '4'. For scale reference, the dimensions of each dark bar next to digit '4' are 2 mm × 0.4 mm.

4. Spectral imaging

During relative probe-sample axial translation, each sample location was imaged by a different wavelength at each frame (e.g. Fig. 2), which allowed, after careful image registration, collection of the full reflected spectrum. To demonstrate spectral imaging within a cylindrical lumen, our probe was advanced through a color printed target (Fig. 3(a)) that was rolled into a 4.5-mm-diameter cylinder. The processes of scanning and data acquisition were

#254022 Received 16 Nov 2015; revised 27 Dec 2015; accepted 4 Jan 2016; published 8 Jan 2016

identical to those in gray-scale imaging, hence, field of view and resolution were similar. Selected frames from a fly-through movie (Visualization 3, Fig. 3(a)) show high reflections whenever the local encoding wavelengths matched the color of the printed pattern; note the contrast drop in the red digit '3' and the bars next to it as they reach the outermost circular region toward the end of the movie. Using the sequentially acquired frames, the total reflected spectra from each color pattern was measured by manually segmenting the patterns (Fig. 3(a), arrows) and calculating their averaged (25 × 25 pixel regions) brightness within each frame. The wavelength corresponding to each spatial location in the frames was calculated using the grating equation and the known optical configuration of the probe. The local spectra of the blue, green, and red digits and squares are shown in Fig. 3(b) by dashed and dotted lines with the corresponding spectra (solid lines) measured using a commercial spectrometer (USB2000+ , Ocean Optics). Each spectrum was normalized by a reference

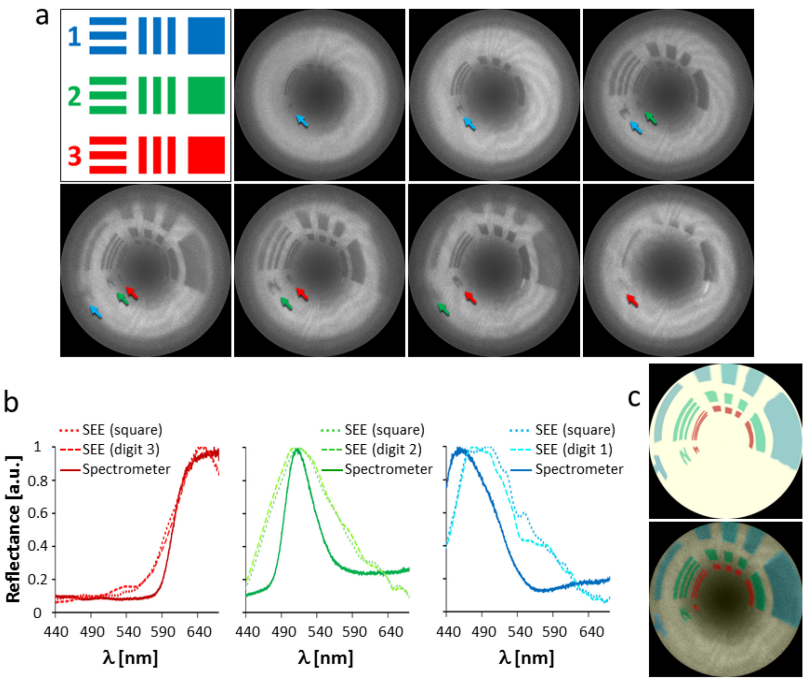

Fig. 3. (a) A series of images from the SEE forward-viewing probe within a cylindrical color target (top-left panel). Axial step size between each frame (left to right, top to bottom) was 2.1 mm. For scale reference, the dimensions of each individual bar next to the digits are 2.3 mm × 0.46 mm. (b) Measured spectra from the different color patterns in (a). Solid lines represent spectra measured by a commercial spectrometer. (c) A reconstructed color image (top panel) and an overlay of the color on a reflectance image (bottom panel).

spectrum captured from the white-color background of the target. For deriving the apparent color of the patterns, each individual pattern was segmented, and its averaged monochromatic reflectivity $r(x(\lambda),y)$ was recorded for each frame of the movie. The spectral reflectivity at each point was converted to the CIE 1931 tristimulus values *XYZ* using the CIE standard observer color matching function $\bar{x}$, $\bar{y}$, and $\bar{z}$ [21]. The CIE *XYZ* values were then converted to linear *RGB* values [22], followed by gamma correction to obtain the standard *RGB* (*sRGB*) values. A color image (Fig. 3(c), top panel) was reconstructed using the calculated sRGB values; an overlay of the measured colors on a selected grayscale image from the original movie is shown at the bottom panel of Fig. 3(c). The color at the dark center region of the image was interpolated to obtain continuous color coverage. Note the slight

#254022 Received 16 Nov 2015; revised 27 Dec 2015; accepted 4 Jan 2016; published 8 Jan 2016

yellow hue of the white background due to the lack of blue wavelengths below 440 nm in the reflected spectra.

In order to demonstrate spectral imaging of a biological tissue, the probe was inserted into an artery that was dissected from a healthy turkey heart (Fig. 4(a)). Selected frames from the acquired movie (Visualization 4), shown in Fig. 4(a), reveal a local tissue damage (labeled 'D'), a black ink spot that was injected into the artery wall (labeled 'I'), and a local burn caused by a hot needle (labeled 'B'). Most noticeable in these images, however, are two dark rings that were observed at the same image location throughout the movie, despite the forward motion of the probe through the artery. An averaged reflection spectrum (Fig. 4(b), squares) from the artery walls shows two reflection minima at approximately 540 nm and 570 nm (marked by green and red arrows in Fig. 4(a)), which correspond to the familiar absorption maxima at the spectrum of oxyhemoglobin (Fig. 4(b), gray solid line [23].). Spectral measurement of the artery wall using a commercial spectrometer is shown in Fig. 4(b) by a black solid line, for reference.

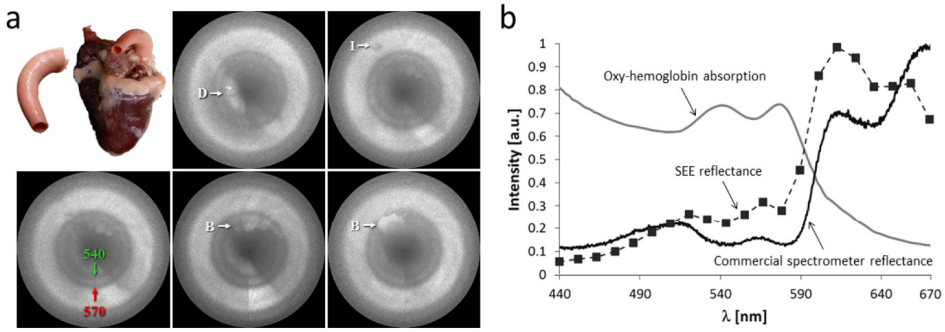

Fig. 4. (a) Turkey artery (top-left panel) imaging using SEE. D – tissue damage; I - ink spot; B - burned tissue. Green and red arrows mark the high absorption rings around 540 nm and 570 nm. The diameter of the ink spot (I) is approximately 1 mm. (b) Averaged artery reflectance spectrum (squares) measured from 21 frames, compared to the oxyhemoglobin absorption spectrum (gray solid line) from Ref [23] and a reflectance spectrum measured by a commercial spectrometer (black solid line).

5. Discussion

The unique forward-viewing angle and rotational scanning of the prototype endoscopic probe enable effective imaging of the inner walls of a lumen while maintaining visual contact along its axis. The tradeoffs of this large field of view include optical aberrations and resolution drop at the inner and outermost regions of the field, and notable scale variation across the field of view. While these aberrations could be tolerable for a standard clinical endoscopic procedure, they make color and spectral imaging challenging due to the difficulty to employ an automatic algorithm that tracks visible features or specific sample locations for recording the narrowband reflections. Future implementation of this probe for spectral imaging would require sophisticated software that tracks specific features despite continuous change in the relative scale, resolution and brightness. Before such software is developed, local spectra could be measured manually by the operator for investigating specific regions of interest.

The use of a two-fiber probe also involves some challenges, mainly the inability to use a conventional optical rotary joint; commercially available rotary joints for multiple channel coupling are often expensive and suffer from high insertion losses, particularly for small core fibers. In our current system, the rotational scanning mechanism rotates the two optical fibers and coils them around the rigid tube (see Visualization 1), which limits the number of unidirectional rotations and necessitates a back and forth rotations. Using a bidirectional coil (the three-layer torque coil from Asahi Intecc Co., for example) would provide a better

#254022 Received 16 Nov 2015; revised 27 Dec 2015; accepted 4 Jan 2016; published 8 Jan 2016

flexibility in a future probe, allowing efficient torque transmission while navigating inside narrow ducts.

Finally, spectral imaging within an *ex-vivo* artery has demonstrated the potential of the system for functional imaging of tissue. Blood oxygenation levels could be computed for each sample location by analyzing the contrast of the oxyhemoglobin absorption peaks, and would be useful for diagnosing various pathologies such as local infections and small tumors. For color imaging, however, our spectral data was less effective for object with blue-color features as these wavelengths were used to encode only axial locations. Future version of the probe could address this issue either by shifting the blue (400 nm - 450 nm) wavelengths away from the optical axis (and thus preventing true forward viewing angles), or by using wavelengths between 360 nm and 400 nm to encode the forward direction.

In summary, a prototype of a forward-viewing SEE probe was demonstrated suitable for imaging within cylindrical geometries such as narrow ducts and vessels. The system is able to measure local reflection spectra, which could be useful for distinguishing between different tissue types based on their unique spectral signature.

Acknowledgments

The study was funded in part by the Israel Science Foundation grant (651/14). This work was also supported in part by the Lorry I. Lokey Interdisciplinary Center for Life Sciences and Engineering.

#254022 Received 16 Nov 2015; revised 27 Dec 2015; accepted 4 Jan 2016; published 8 Jan 2016